ACSNANO

www.acsnano.org

ARTICLE

# Characterization of Excitonic Nature in Raman Spectra Using Circularly Polarized Light

Yan Zhao, Shishu Zhang, Yuping Shi, Yanfeng Zhang, Riichiro Saito, Jin Zhang, and Lianming Tong*

Cite This: *ACS Nano* 2020, 14, 10527−10535

Read Online

ACCESS | Metrics & More | Article Recommendations | Supporting Information

**ABSTRACT:** We propose a technique of Raman spectroscopy to characterize the excitonic nature and to evaluate the relative contribution of the two kinds of electron/exciton−phonon interactions that are observed in two-dimensional transition-metal dichalcogenides (TMDCs). In the TMDCs, the electron/exciton−phonon interactions mainly originate from the deformation potential (DP) or the Fröhlich interaction (FI) which give the mutually different Raman tensors. Using a circularly polarized light, the relative proportion of the DP and the FI can be defined by the ratio of helicity-polarized intensity that is observed by $MoS_2$. By this analysis, we show that the excitonic FI interaction gradually increases with decreasing temperature, contributes equally to DP at ∼230 K, and dominates at lower temperatures. The excitonic effect in the Raman spectra is confirmed by modulating the dielectric environment for the exciton and by changing the laser power.

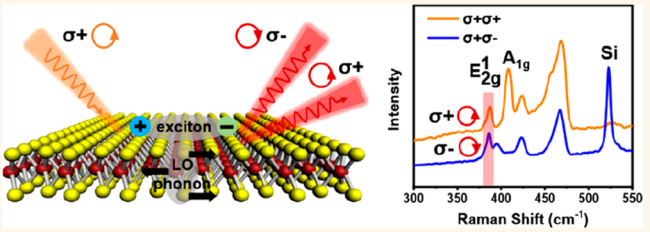


**KEYWORDS:** *exciton−phonon coupling, circularly polarized light, Raman scattering, $MoS_2$, helicity, deformation potential, Fröhlich interaction*

Raman spectroscopy has been a useful technique for the characterization of two-dimensional (2D) transition metal dichalcogenides (TMDCs).[1−5] In the polarized Raman spectra, the electron−phonon (or exciton−phonon) coupling gives phonon-mode specific angle-dependence of the Raman spectra that are determined by the Raman tensor.[6−8] In 2D TMDCs, the electron− or exciton−phonon interaction originates mainly from the deformation potential (DP) and the Fröhlich interaction (FI).[9−11] For the DP, the volume-changing lattice vibration modifies the crystal potential that induces an inelastic scattering of an electron by emitting (or absorbing) a phonon.[12] The FI refers to the interaction between the electrons/excitons and the longitudinal optical (LO) phonons in polar or ionic crystals which can generate a macroscopic electric field because of the out-of-phase motion for adjacent atoms.[13] However, the relative contribution of the two origins of interaction cannot be characterized by conventional Raman spectroscopy. Here, we propose a technique to evaluate the relative contribution by using circularly polarized Raman spectroscopy, based on the fact that the DP and the FI give the mutually different Raman tensors in the polarized Raman spectra.[14−17]

Since the circularly polarized light has a spin angular momentum + $\hbar$ or − $\hbar$ of a photon, the optical transition in the 2D TMDCs occurs at one of the two valleys, K or K′ in the hexagonal Brillouin zone, which is known as the valley-polarized optical transition.[18,19] For Raman active modes excited by circularly polarized light, the helicity of scattered light can be changed or conserved depending on the helicity selection rule.[20−22] For example, the $E^1_{2g}$ mode of $MoS_2$ is helicity-changed in which the angular momentum of the light is conserved in the Raman process,[20,23] and the selection rule is determined by the Raman tensor corresponding to the DP. However, when the optical transition is given by the exciton of the 2D material for the laser excitation energy resonant to the excitonic energy, the FI can be much stronger than DP,[24] which makes the $E^1_{2g}$ mode helicity-conserved. In the Raman scattering process, the relative strength of the DP to the FI can be estimated experimentally by the relative Raman intensity of the helicity-changed to helicity-conserved components. Martin pointed out that both electron−phonon and exciton−phonon interactions exist in the DP or the FI, and the proportion of electron/exciton−phonon interactions in the DP or the FI depends on the excitation energy.[24] For off-excitonic resonance excitation, the electron−phonon interaction dominates and the strength of electron−phonon interaction for the DP can be much larger than that for the FI. Whereas for on-excitonic

Received: May 29, 2020
Accepted: August 10, 2020
Published: August 10, 2020






https://dx.doi.org/10.1021/acsnano.0c04467
*ACS Nano* 2020, 14, 10527−10535

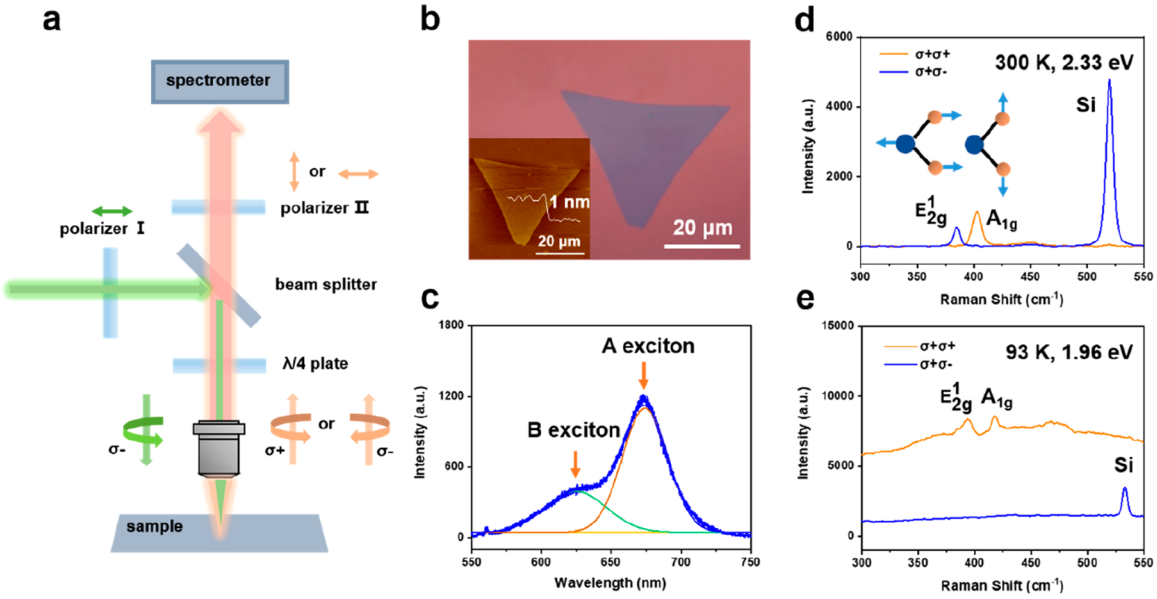


**Figure 1. Helicity-resolved Raman spectra of monolayer $MoS_2$ for on- and off-excitonic resonance excitations. (a) Schematic diagram of the experimental setup for helicity-resolved Raman spectroscopy. (b) Optical image of CVD-grown monolayer $MoS_2$. Inset shows the AFM image of the $MoS_2$ flake, of which the thickness is 1 nm. (c) Photoluminescence (PL) spectrum of monolayer $MoS_2$ excited by 2.33 eV (532 nm) laser fitted by Gaussian functions. The peaks at 674 nm (1.84 eV) and 625 nm (1.98 eV) correspond to the A and B excitons, respectively. (d, e) Helicity-resolved Raman spectra of monolayer $MoS_2$ excited by (d) 2.33 eV (532 nm) at 300 K and (e) 1.96 eV (633 nm) at 93 K. The inset in (d) shows the atomic vibrations of the $E^1_{2g}$ and $A_{1g}$ modes.**

resonance excitation, the exciton−phonon interaction can be dominant and the FI can be stronger than the DP.[14,24]

In order to confirm the excitonic effect on the relative intensities of the FI and the DP, we have measured the helicity-resolved Raman spectra of $MoS_2$ as a function of temperature by on-excitonic resonance excitation. The relative contribution of the DP to the FI is estimated by the helicity polarization ratio of the $E^1_{2g}$ mode, and the increase of the FI at lower temperatures indicates the enhancement of the excitonic effect. Further, we modulated the dielectric environment of excitons by constructing h-BN/$MoS_2$ heterostructure or depositing $HfO_2$ on the surface of $MoS_2$, and we find that the Raman intensity contributed by the DP does not depend much on the dielectric constant while the contribution of the FI decreases with increasing the dielectric constant due to the reduction of exciton binding energy by dielectric screening. Further, we explored the influence of layer number and laser power on the helicity polarization ratio, and all measurements give a consistent picture of the excitonic nature in Raman spectra. The present technique of Raman spectroscopy is important for the characterization of exciton photophysics in the 2D materials and for exploring the evolution of different exciton−phonon couplings.

## RESULTS AND DISCUSSION

**Helicity-Resolved Raman Spectroscopy of $MoS_2$.** The experimental setup of helicity-resolved Raman spectroscopy is shown in Figure 1a. The incident laser passes through the linear polarizer and the quarter-wave plate to produce a left ($\sigma+$) or right ($\sigma-$) circularly polarized light which we call $\sigma+$ or $\sigma-$ helicity of circularly polarized light. The Raman-scattered light passes through the quarter-wave plate again and another linear polarizer for selecting the helicity of the scattered light. If the helicity of the scattered light $\sigma_s$ is the same as the incident one $\sigma_i$, that is, $(\sigma_s\sigma_i) = (\sigma+\sigma+)$ or $(\sigma-\sigma-)$, it is termed as helicity-conserved scattering. In this case, the Raman signal will be the strongest (zero) for the $\sigma+\sigma+$ ($\sigma+\sigma-$) configuration. If $\sigma_s$ and $\sigma_i$ are opposite, such as ($\sigma+\sigma-$) or ($\sigma-\sigma+$), it is a helicity-changed scattering. In this case, the Raman signal will be zero (strongest) for the $\sigma+\sigma+$ ($\sigma+\sigma-$) configuration.

$MoS_2$ belongs to a hexagonal crystal family, and the point group of the unit cell for bulk $MoS_2$ is $D_{6h}$.[25] $MoS_2$ with odd number of layers lacks inversion symmetry and belongs to $D_{3h}$ point group, while $MoS_2$ with even number of layers has inversion symmetry and belongs to the $D_{3d}$ point group. The sample of monolayer $MoS_2$ used in the present experiment is prepared by chemical vapor deposition (CVD) method and the sample is transferred onto 300 nm $SiO_2$/Si substrate, as shown in Figure 1b. The growth and transfer processes are given in the experimental Methods. Atomic force microscope (AFM) measurements show the thickness of 1 nm for the $MoS_2$ flake, consistent with being a monolayer.

Monolayer $MoS_2$ has a direct bandgap around 1.9 eV with split valence bands (~148 meV) at the K point of the Brillouin zone due to the spin−orbit coupling.[26] Thus, there are two main peaks in the photoluminescence (PL) spectrum corresponding to the direct transitions of A, B excitons,[27] respectively. The measured PL spectrum of the monolayer $MoS_2$ is shown in Figure 1c, where the A and B excitons appear at 674 nm (1.84 eV) and 625 nm (1.98 eV), respectively. The helicity-resolved Raman spectra of the monolayer $MoS_2$ are measured for 2.33 eV (532 nm) and 1.96 eV (633 nm) laser excitation energies ($9E_L$).

There are two first-order Raman active modes for $MoS_2$ which are measured in the backscattering geometry, that is, $E^1_{2g}$ and $A_{1g}$ modes. The $E^1_{2g}$ mode is an in-plane vibration of Mo and S atoms and is a doubly degenerate mode of the LO/TO phonons at the Γ point of Brillouin zone. The $A_{1g}$ mode comes from the ZO phonon and is an out-of-plane vibration of S


https://dx.doi.org/10.1021/acsnano.0c04467
ACS Nano 2020, 14, 10527−10535

atoms.[28] In Figure 1d, the helicity-resolved Raman spectra that are measured at $T$ = 300 K for the off-resonant condition ($E_L$ = 2.33 eV) show that the $E^1_{2g}$ mode appears at 384 $cm^{-1}$ for the $\sigma+\sigma-$ configuration (blue line), which means that the $E^1_{2g}$ mode is helicity-changed Raman scattering, which is consistent with the Raman tensor for the DP of the $E^1_{2g}$ mode. Tatsumi et al. have reported the helicity selection rule for $E^1_{2g}$ mode by the conservation law of pseudoangular momentum (PAM),[23] which is given by $\sigma_s - \sigma_i = -m_v^{ph} + N_V p$, where $\sigma_i$ and $\sigma_s$ are the angular momentums of the incident and scattered photons, respectively, $m_v^{ph}$ is the PAM of the phonon, $N_V$ is the rotational symmetry of the vibration mode, and $p$ is an arbitrary integer. For $m_v^{ph}$, Zhang et al. have reported that the phonons at high symmetry points (Γ, K, K′) of the Brillouin zone for hexagonal lattices are chiral which have a finite PAM.[29] For example, the doubly degenerate $E^1_{2g}$ mode of $MoS_2$ has a PAM of $\pm\hbar$ which is equivalent to $\mp 2\hbar$ for the 3-fold rotational symmetry of the crystal, corresponding to the selection rule for the helicity-changed $E^1_{2g}$ mode.[29] On the other hand, the $A_{1g}$ mode appears at 403 $cm^{-1}$ for the $\sigma+\sigma+$ configuration (orange line), which means that the $A_{1g}$ mode is helicity-conserved Raman scattering, which is also consistent with the previous works.[20] It is worth noting that the peak at 520 $cm^{-1}$ ($T_{2g}$ mode) due to the silicon substrate is also helicity-changed Raman scattering. The helicity selection rule for these peaks are given by the Raman tensor analysis in Notes S1 and S2.

In Figure 1e, we show Raman spectra at $T$ = 93 K for the resonant condition $E_L$ = 1.96 eV. Since the Raman intensity of monolayer $MoS_2$ at $T$ = 300 K excited by the 1.96 eV laser is too weak to distinguish because of the accompanying strong PL background, the helicity-resolved Raman spectra are measured at a low temperature (93 K), at which the intensities of $E^1_{2g}$ and $A_{1g}$ modes are enhanced, as will be discussed later. As shown in Figure 1e, although the second-order Raman modes are still too weak to be seen here, there are two obvious first-order Raman peaks in the resonance Raman spectra. However, compared with that in Figure 1d, the helicity selection rule changes. The $A_{1g}$ mode remains helicity-conserved, whereas the $E^1_{2g}$ mode changes from helicity-changed to helicity-conserved. In fact, the $E^1_{2g}$ mode appears for the $\sigma+\sigma+$ configuration and the signal for the $\sigma+\sigma-$ configuration almost disappears.

This phenomenon can be explained by the fact that the LO phonons at the resonant condition interact with excitons mainly by the FI.[14,17] The helicity selection rule can be determined by the Raman tensor, which involves the symmetry of crystal structure and vibration modes.[20,21,23,30] The calculated Raman intensity is determined by $I \propto |\sigma_s^{\dagger}\cdot R\cdot\sigma_i|^2$, where $R$ is the Raman tensor, $\sigma_s$ and $\sigma_i$ are the helicities of the scattered and incident circularly polarized light denoted by the Jones vectors. For example, for left-handed circular polarization, $\sigma+ = \frac{1}{\sqrt{2}}\begin{pmatrix}1\\ i\\ 0\end{pmatrix}$, and for right-handed circular polarization, $\sigma- = \frac{1}{\sqrt{2}}\begin{pmatrix}1\\ 0\\ i\end{pmatrix}$. The Raman tensors for the $E^1_{2g}$ mode that include both DP and FI are expressed by[15−17,31]

$$R_{LO} = \begin{pmatrix} a_F & a_{DP} & 0 \\ a_{DP} & a_F & 0 \\ 0 & 0 & a_F \end{pmatrix}, \quad R_{TO} = \begin{pmatrix} a_{DP} & 0 & 0 \\ 0 & -a_{DP} & 0 \\ 0 & 0 & 0 \end{pmatrix} \qquad (1)$$

where $a_F$ and $a_{DP}$ are the elements corresponding to the FI and the DP, respectively. Thus, the Raman intensities of the $E^1_{2g}$ mode for the $\sigma+\sigma+$ and $\sigma+\sigma-$ configurations are $I_{\sigma+\sigma+} \propto |a_F|^2$ and $I_{\sigma+\sigma-} \propto |a_{DP}|^2$, corresponding to the contributions *via* the FI and the DP, respectively. The detailed calculations are given in Note S1. The calculations directly explain the results in Figure 1d,e that the DP is dominant for off-resonant 2.33 eV excitation, while the FI is the major component of exciton−phonon coupling for resonant 1.96 eV excitation. Thus, the helicity-resolved Raman spectra show intuitively the proportion of the two kinds of exciton−phonon interactions, which cannot be reflected in the Raman spectra without light polarization (Figure S1).

As can be compared with the PL spectrum in Figure 1c, $E_L$ = 1.96 eV corresponds to being resonant to the A-exciton and partly to the B-exciton. As a result, more excitons can be formed for $E_L$ = 1.96 eV than 2.33 eV, and the exciton couples to a phonon in the Raman scattering process (Figure 2a), while

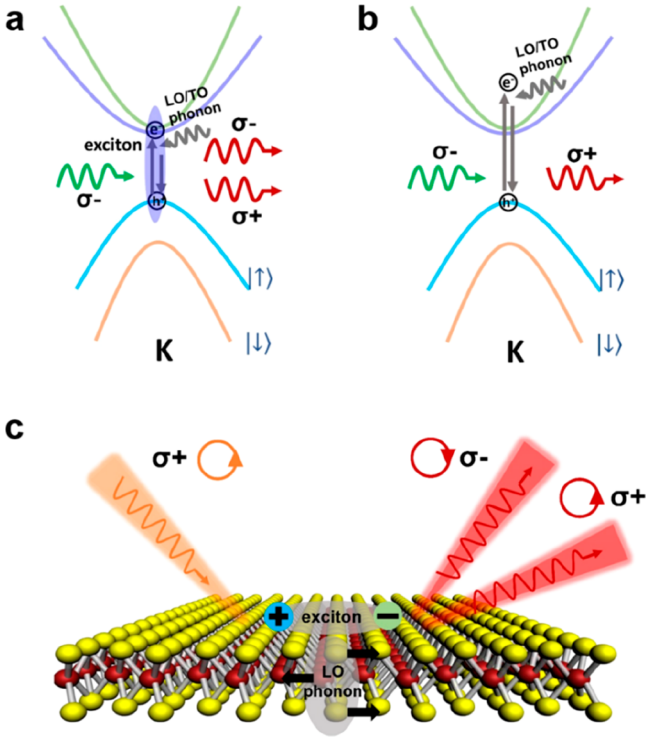


**Figure 2. Schematics of the coupling of electron- or exciton−phonon and the helicity selection rule for Raman scattering in $MoS_2$. (a, b) Schematic of the Raman scattering processes for monolayer $MoS_2$ excited by circularly polarized light with specific helicity and the helicities of the Raman scattering light for (a) on- and (b) off-excitonic resonance excitations. (c) Illustration of the coupling of LO phonon and exciton in $MoS_2$. Black arrows indicate the vibration directions of Mo and S atoms for LO phonon.**

for $E_L$ = 2.33 eV excitation, there form mainly free electron−hole pairs and the electrons or holes interact with the phonons (Figure 2b). Although both the DP and the FI exist for a general $E_L$, the FI is enhanced much more than the DP for the resonant condition.[24] The Raman processes and helicity selection rules of the $E^1_{2g}$ mode for on- and off-excitonic resonance excitations by circularly polarized light are schematically shown in Figure 2a,b, respectively. For the on-excitonic resonance excitation by right-handed circularly polarized light as shown in Figure 2a, the excitons at the K valley are excited


https://dx.doi.org/10.1021/acsnano.0c04467
ACS Nano 2020, 14, 10527−10535

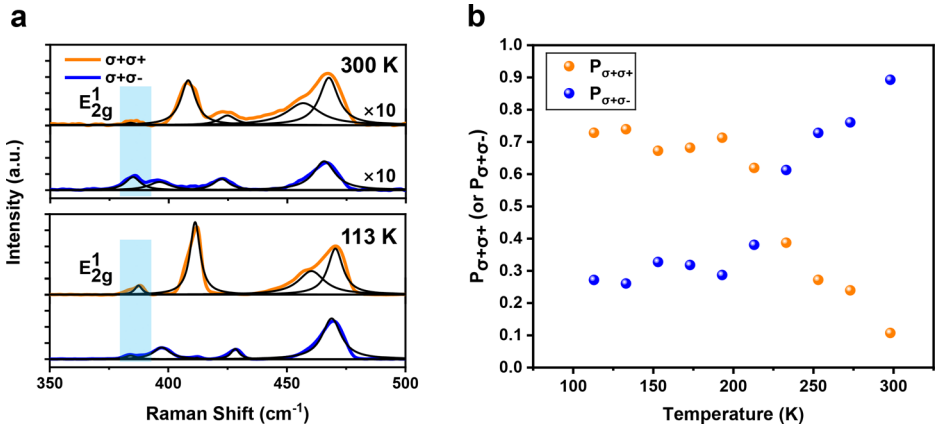


**Figure 3. Exciton−phonon coupling *via* the DP and the FI at different temperatures. (a) Helicity-resolved Raman spectra of $MoS_2$ at 300 and 113 K. The assignment of the Raman peaks appeared here are shown in Figure S6 and Table S1. (b) Proportions of helicity-conserved ($P_{\sigma+\sigma+}$) and helicity-changed ($P_{\sigma+\sigma-}$) components of the $E^1_{2g}$ mode as a function of temperature.**

and the emitted photons from the K valley are mainly helicity-conserved according to the valley-optical selection rule.[18,19] However, for the inelastic-scattered photons by one-phonon Raman scattering that occurs within the same valley, the helicity of the scattered light for the LO/TO phonons at the Γ point can be helicity-changed or helicity-conserved depending on the DP or FI, respectively, although the helicity-changed Raman process can be somewhat suppressed by the valley polarization when the excitation energy is close to the energy gap at the K point.[30]

As the term $a_F$ appears in the diagonal elements in the Raman tensor of LO mode as shown in eq 1, $a_F$ affects the Raman scattering selection rule for the σ+σ+ configuration. For example, the enhancement of the forbidden 1LO phonon scattering in CdS near the excitonic resonance is attributed to the strong FI.[14] As shown in Figure S2, the change of Raman tensor can be clearly observed by the Raman spectra using linearly polarized light of $MoS_2$ for the off- and on-excitonic resonance excitation. In this case, the intensities of the $E^1_{2g}$ mode for the XX (∥) and XY (⊥) configurations are $I_{\parallel} \propto |a_F|^2 + |a_{DP}|^2$and $I_{\perp} \propto |a_{DP}|^2$, respectively (Note S3). For the off-resonant condition, $I_{\parallel}$ and $I_{\perp}$a re approximately the same since the contribution of the FI is small compared with the DP. However, for the on-excitonic resonance condition, since the FI component is dominant, $I_{\parallel}$ becomes much stronger than $I_{\perp}$, which is consistent with the results using circularly polarized light.

**Strength of Exciton−Phonon Coupling *via* the DP and the FI in $MoS_2$.** In a resonant Raman scattering process, the Raman cross sections corresponding to contributions of the DP and the FI are calculated theoretically.[15] The strength expressions of the DP and the FI are shown in Note S4. It is seen that the coupling strength of the FI is $1/q$ dependent where $q$ is a wave vector for a phonon. The $E^1_{2g}$ mode corresponds to the zone-center LO phonon at Γ-point with $q \approx 0$; thus, the strength of the FI can be expected to be large for a small $q$.[11]

First-principle calculations have shown that, for off-resonant conditions, the electron−phonon interaction of the DP for the TO phonon at Γ-point has a value of 4 eV.[10] On the other hand, the electron−phonon interaction of the FI is approximately 98 meV for the LO phonon at Γ point in single layer $MoS_2$,[10] which is much weaker than that of the DP. That is the reason why the helicity-conserved component of the $E^1_{2g}$ mode for off-resonant condition is hardly observed. However, for the on-excitonic resonance condition, the contribution of the FI can be comparable or even much stronger than the DP and the strengths of the DP and the FI exhibit different sensitivities to the excitonic effect,[14,24] which will be discussed in detail in the next section. In Figure 2c, we illustrate the schematic diagram of the exciton-LO phonon coupling in $MoS_2$ and the corresponding helicity selection rule for the Raman scattering.

According to the selection rule of helicity-resolved Raman scattering, the Raman intensities for the σ+σ+ and σ+σ− configurations represent the coupling strengths of the FI and the DP, and the proportions of the FI and the DP can then be defined by

$$P_{\sigma+\sigma+} = \frac{I_{\sigma+\sigma+}}{I_{\sigma+\sigma+} + I_{\sigma+\sigma-}} = \frac{|a_F|^2}{|a_F|^2 + 2|a_{DP}|^2},$$
$$P_{\sigma+\sigma-} = 1 - P_{\sigma+\sigma+} = \frac{2|a_{DP}|^2}{|a_F|^2 + 2|a_{DP}|^2} \quad (2)$$

respectively. Besides, the relative proportion of the DP and the FI can be defined by the helicity polarization ratio:

$$\rho = \frac{I_{\sigma+\sigma+} - I_{\sigma+\sigma-}}{I_{\sigma+\sigma+} + I_{\sigma+\sigma-}} \quad (3)$$

**Evaluating the DP and the FI Contributions in $MoS_2$ at Different Temperatures.** In order to evaluate $P_{\sigma+\sigma+}$ and $P_{\sigma+\sigma-}$ in eq 2, we measured the helicity-resolved Raman spectra of multilayer $MoS_2$ excited by $E_L$ = 1.96 eV as a function of temperature ranging from 113 to 300 K. In Figure 3a, we show the Raman spectra for the σ+σ+ (orange line) and σ+σ− (blue line) configurations at 113 and 300 K, respectively. It is worth noting that the total Raman intensity of $MoS_2$ at 113 K is much larger than that at room temperature, and the intensity of the $A_{1g}$ mode as a function of temperature is shown in Figure S3. The reason why the total Raman intensity is large at the low temperature is that a photoexcited electron and a hole can bind to an exciton easily at low temperature and that the exciton−photon matrix element is dominant compared with electron−photon matrix element. Another possible reason is that the exciton energy level becomes closer to the excitation laser with decreasing temperature and the resonance enhancement becomes larger.[32,33] The Raman intensities of the


https://dx.doi.org/10.1021/acsnano.0c04467
ACS Nano 2020, 14, 10527−10535

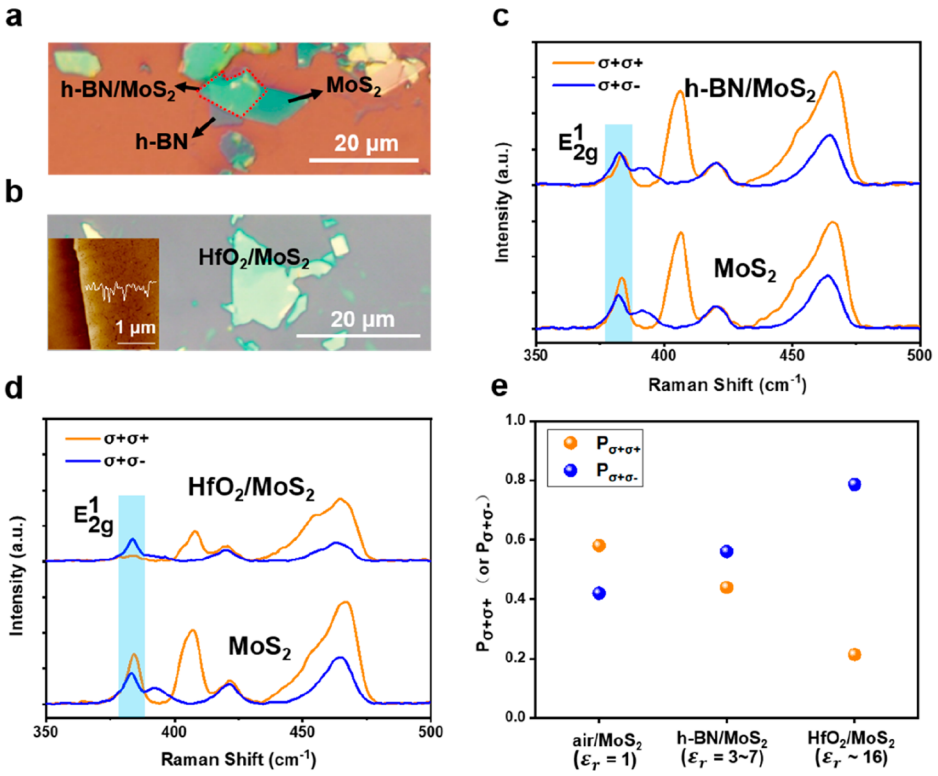


**Figure 4. Dielectric modulation of exciton−phonon interaction. (a) Optical image of h-BN/$MoS_2$ heterostructure. (b) Optical image of mechanically exfoliated $MoS_2$ flake covered by 10 nm $HfO_2$ which is deposited by ALD. The inset shows the AFM image of the $MoS_2$ flake covered by $HfO_2$, where the roughness profile indicates the relative uniformity of the $HfO_2$ layer. (c) Helicity-resolved Raman spectra of bare $MoS_2$ and $MoS_2$ covered by BN, excited by 1.96 eV laser. (d) Helicity-resolved Raman spectra of bare $MoS_2$ and $MoS_2$ covered by $HfO_2$, excited by 1.96 eV laser. (e) Proportions of helicity-conserved ($P_{\sigma+\sigma+}$) and helicity-changed ($P_{\sigma+\sigma-}$) Raman scattering for air/$MoS_2$, h-BN/$MoS_2$ and $HfO_2$/$MoS_2$. $\varepsilon_r$ = 1, 3−7 and ∼16 correspond to the relative dielectric constant of air, h-BN and $HfO_2$, respectively.**

$E^1_{2g}$mode for the $\sigma+\sigma+$ and $\sigma+\sigma-$ configurations as a function of temperature are shown in Figure S4, which clearly show the increase of the DP and FI with decreasing temperature.

The helicity polarization ratio of $A_{1g}$ mode remains constant (Figure S5), whereas the helicity of the $E^1_{2g}$ mode changes with the temperature. In Figure 3b, we plot the values of $P_{\sigma+\sigma+}$ and $P_{\sigma+\sigma-}$ of the $E^1_{2g}$ mode from $T$ = 113 to 300 K. As shown in Figure 3b, the proportion of helicity-changed component determined by the DP increases, while the proportion of helicity-conserved component determined by the FI decreases with increasing temperature, and they are equal at approximately 230 K. This means that the excitonic FI gradually increases with decreasing temperature, contributes equally to the DP at ∼230 K, and dominates at lower temperatures.

The exciton−phonon coupling by the FI is enhanced when $E_L$ is matched to the exciton energy, as has been shown in CdS.[24] The decrease of temperature results in the approach of exciton energy to the excitation energy;[32,33] thus, both the FI and the DP are enhanced. However, the FI is enhanced much more than the DP, which is consistent with the theory reported by Martin[24] in which he pointed out that the Raman scattering cross sections determined by the DP and the FI depend on the excitation energy by $\sigma_{DP} \propto (E_g - E_L)^{-1}$ and $\sigma_{FI} \propto (E_g - E_L)^{-3}$, respectively, where $E_g$ is the band gap and $E_L$ is the laser excitation energy. Thus, the Raman intensity determined by the FI increases more rapidly than the DP near excitonic resonance.

**Dielectric Modulated Exciton−Phonon Coupling.** In order to confirm the excitonic nature of Raman spectra, we tune the excitonic energy by changing the dielectric constant. The dielectric environment can affect the exciton binding energy due to the Coulomb screening,[34−36] and when the dielectric constant increases, the exciton becomes delocalized in the real space. The detailed discussion on dielectric screening on excitons is given in Note S5. It is noted here that the exciton−phonon interaction *via* the DP is not so sensitive to the dielectric function since the DP is defined by much smaller size than the exciton size and, thus, the exciton−phonon matrix element would give a value similar to that of the electron−phonon matrix element.[37,38] The modulated coupling strength of the exciton−phonon can be monitored by the helicity-resolved Raman scattering.

In Figure 4a,b, we show the optical images of $MoS_2$ covered by few-layer h-BN (the relative dielectric constant $\varepsilon_r$ is approximately 3−7[39]) and 10 nm $HfO_2$ ($\varepsilon_r \approx 16$[40]). The thickness of h-BN is 11 nm, as shown in Figure S7. The inset in Figure 4b shows the AFM image of a $MoS_2$ flake partially covered by $HfO_2$, which is deposited by the Atomic Layer Deposition (ALD) method, and the roughness profile indicates the relative uniformity of the $HfO_2$ layer. In Figure 4c,d, we plot the corresponding helicity-resolved Raman spectra for resonant $E_L$ = 1.96 eV. The helicity polarization ratio of the $A_{1g}$ mode does not change with the dielectric environment (Figure S8), whereas the relative intensities of the $E^1_{2g}$ mode in $\sigma+\sigma+$ and $\sigma+\sigma-$ configurations change obviously. The intensities of the $E^1_{2g}$ mode in the two configurations are extracted for bare $MoS_2$ (air/$MoS_2$), $MoS_2$ covered by h-BN (h-BN/$MoS_2$), and $MoS_2$ covered by $HfO_2$ ($HfO_2$/$MoS_2$), as shown in Figure S9.


https://dx.doi.org/10.1021/acsnano.0c04467
ACS Nano 2020, 14, 10527−10535

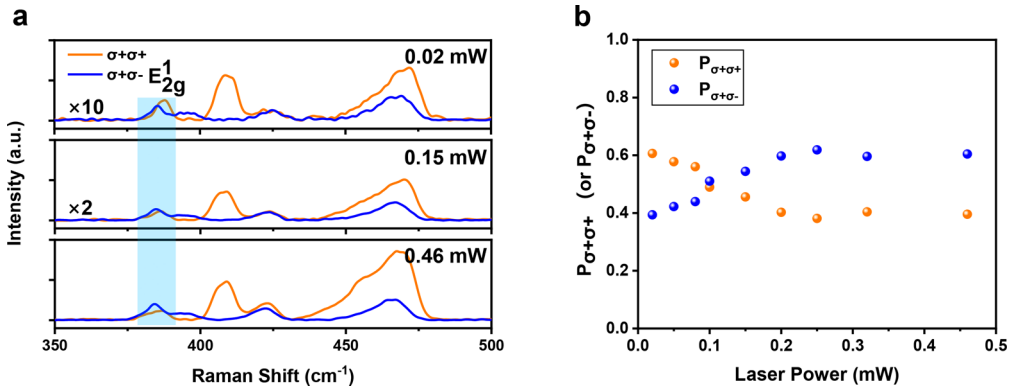


**Figure 5. Exciton−phonon interaction *via* the DP and the FI at different laser powers. (a) Helicity-resolved Raman spectra of $MoS_2$ excited by 1.96 eV laser with the powers of 0.02 mW, 0.15 mW and 0.46 mW, respectively. (b) Proportions of helicity-conserved ($P_{σ+σ+}$) and helicity-changed ($P_{σ+σ−}$) Raman scattering with the variation of laser power.**

With the increase of dielectric constant, the helicity-changed component determined by DP shows little change, whereas the helicity-conserved component determined by FI decreases obviously. The proportions of helicity-conserved ($P_{σ+σ+}$) and helicity-changed ($P_{σ+σ−}$) Raman scattering are calculated and plotted in Figure 4e, which clearly shows the decrease of the FI contribution with increasing the dielectric constant.

**Strength of Exciton−Phonon Coupling in $MoS_2$ Affected by Layer Number and Laser Power.** Finally, we discuss the layer number dependence and laser power dependence for the exciton−phonon coupling. The measured helicity-resolved Raman spectra and the extracted helicity polarization ratios of $MoS_2$ for several layer numbers are shown in Figure S10 and Figure S11, respectively. As shown in Figure S11, $\rho$ decreases with increasing layer number, which indicates the decrease of the FI with increasing layer number. This can be attributed to the increase of dielectric constant for multilayer $MoS_2$.[41] When the layer number increases, the dielectric screening effect on the excitons becomes stronger and the exciton binding energy decreases,[36] which accounts for the weakening of exciton−phonon coupling *via* the FI, consistent with reported theoretical models.[11]

In Figure 5, we show the laser power dependence of the coupling strength of exciton−phonon *via* the FI and the DP for $E_L$ = 1.96 eV, and the laser power ranges from 0.02 mW ($2.5 \times 10^3$ W/cm$^2$) to 0.46 mW ($5.9 \times 10^4$ W/cm$^2$). To avoid the thermal damage of the sample, the laser power is kept below 0.5 mW. In Figure 5a, we show the helicity-resolved Raman spectra excited by laser powers of 0.02, 0.15, and 0.46 mW. The change of laser power has no influence on the helicity selection rule of the $A_{1g}$ mode (Figure S12). At 0.02 mW, the helicity-conserved component ($\sigma+\sigma+$) of the $E^1_{2g}$ mode is larger than the helicity-changed ($\sigma+\sigma-$) component, but the relative intensity of helicity-conserved component decreases with increasing the laser power.

The calculated $P_{σ+σ+}$ and $P_{σ+σ−}$ values are shown in Figure 5b. It is clearly seen that the proportion of the FI decreases with increasing laser power, whereas the proportion of the DP increases. This can be explained by the increase of temperature at higher laser powers.[42] The peak positions of the $A_{1g}$ mode with increasing laser power are shown in Figure S13. The relationship between peak shift and temperature can be expressed as $\Delta\omega = A\cdot\Delta T$, where $A$ is the temperature coefficient and is reported to be $-0.011 \pm 0.001$ and $-0.013 \pm 0.001$ cm$^{-1}$/K for the $E^1_{2g}$ and $A_{1g}$ mode, respectively.[43] A redshift of 0.8 cm$^{-1}$ for the $A_{1g}$ mode with the variation of laser power from 0.02 to 0.46 mW is observed, corresponding to the elevation of temperature of $\Delta T \approx 62$ K, which accounts for the decrease of the proportion of the FI. Besides, the effect of charge doping caused by the increase of laser power may also matter,[44] which can suppress the intensity of the FI.[17]

## CONCLUSIONS

The Raman scattering process of the first-order $E^1_{2g}$ mode for on-excitonic resonance excitation involves the exciton-photon interaction and the exciton−phonon interaction for the LO phonons near Γ point *via* both the DP and the FI. Since the helicity selection rule for the DP and the FI are different from each other, the helicity-conserved and helicity-changed components of the $E^1_{2g}$ mode represent the strength of the FI and the DP, respectively, which can be used for evaluating the excitonic nature. Here we utilized the helicity-resolved Raman spectroscopy to evaluate the proportions of the FI and the DP in layered $MoS_2$ by changing (1) laser excitation energy, (2) temperature, (3) dielectric constant of surrounding material, (4) layer number, and (5) laser power. All of the results are consistent with the fact that the exciton binding energy can be tuned, and the excitonic nature can be characterized by helicity-resolved Raman scattering. The evolution of the FI and the DP as a function of temperature is explored, and we show that the FI dominates at lower temperature due to the exciton effect. The dielectric modulation of excitons, and thus the exciton−phonon interaction, is also monitored by helicity-resolved Raman spectroscopy. With the increase of dielectric constant, the exciton binding energy decreases due to the dielectric screening effect on the Coulomb interaction, and the exciton−phonon coupling *via* the FI is weakened much more than the DP, resulting in the change of the proportion of helicity-conserved to helicity-changed Raman intensities of the $E^1_{2g}$ mode. The present work provides a measuring technique for the exploration of electron/exciton−phonon interaction and the characterization of the excitonic nature in 2D semiconductors by helicity-resolved Raman spectroscopy.

## METHODS

**Preparation of $MoS_2$.** The $MoS_2$ samples used here are grown by chemical vapor deposition (CVD) on sapphire or mechanically exfoliated onto 300 nm $Si/SiO_2$ substrate. CVD-grown $MoS_2$ samples on sapphire are then transferred onto the 300 nm $Si/SiO_2$ substrate with the assistance of PMMA.


https://dx.doi.org/10.1021/acsnano.0c04467
ACS Nano 2020, 14, 10527−10535

**Construction of h-BN/$MoS_2$ and $HfO_2$/$MoS_2$ Heterostructure. Construction of h-BN/$MoS_2$ Heterostructure.** The $MoS_2$ and h-BN flakes are first exfoliated onto 300 nm Si/$SiO_2$ substrate and polydimethylsiloxane (PDMS), respectively. Then the $MoS_2$ and h-BN flakes are aligned under an optical microscope. The PDMS is stamped onto the silicon substrate to stack the h-BN on the $MoS_2$ flake. Then the PDMS is removed, and the h-BN/$MoS_2$ heterostructure is obtained on the Si/$SiO_2$ substrate. *Construction of $HfO_2$/$MoS_2$ heterostructure:* Deposition of $HfO_2$ layer on $MoS_2$ flakes is performed in an Atomic Layer Deposition (ALD) system (Cambridge NanoTech, Savannah). Precursor $[(CH_3)_2N]_4Hf$ and $H_2O$ are alternatively introduced into the reactive cavity, and the final thickness of $HfO_2$ is controlled by the counts of pulse circles.

**Raman Scattering and Photoluminescence Spectroscopies.** The Raman scattering and photoluminescence spectroscopic measurements are performed on a confocal Raman spectroscope (JY Horiba HR800) in the backscattering geometry. The laser energies used in this work are 1.96 and 2.33 eV and are focused on the sample by a 100× objective lens (NA = 0.9). The laser power is kept below 0.5 mW to avoid damage to materials. The low-temperature experiment is performed in a cryogenic stage (Linkam LTS420) which is refrigerated by liquid nitrogen.

## ASSOCIATED CONTENT

### Supporting Information

The Supporting Information is available free of charge at https://pubs.acs.org/doi/10.1021/acsnano.0c04467.

Notes S1−S5: The calculation process of the polarization selection rule for the $E^1_{2g}$ mode and $A_{1g}$ mode of $MoS_2$ and the $T_{2g}$ mode of silicon; the expressions for the coupling strength of the FI and the DP; the dielectric screening effect on the exciton. Figures S1−S13, Table S1: comparison between Raman spectra taken with and without the selective collection of the helicity; linear polarization-resolved Raman spectra of $MoS_2$; the intensity of the $A_{1g}$ mode of $MoS_2$ as a function of temperature; Raman intensities of the $E^1_{2g}$ mode under $\sigma+\sigma+$ and $\sigma+\sigma-$ configurations with the variation of temperature; the variation of the helicity polarization ratio of the $A_{1g}$ mode as a function of temperature, dielectric constant and laser power; the peak fitting results and the assignments for the resonant Raman peaks of $MoS_2$; thickness measurement of h-BN used in the heterostructure; the extracted intensities of the $E^1_{2g}$ mode of $MoS_2$ in heterostructures; helicity-resolved Raman spectra and the helicity polarization ratio for $MoS_2$ with different layer numbers; change of peak position for the $A_{1g}$mode as a function of laser power (PDF)

## AUTHOR INFORMATION


### Corresponding Author

**Lianming Tong** − *Center for Nanochemistry, Beijing Science and Engineering Center for Nanocarbons, Beijing National Laboratory for Molecular Sciences, College of Chemistry and Molecular Engineering, Peking University, Beijing 100871, P.R. China;* orcid.org/0000-0001-7771-4077; Email: tonglm@pku.edu.cn

### Authors

**Yan Zhao** − *Academy for Advanced Interdisciplinary Studies and Center for Nanochemistry, Beijing Science and Engineering Center for Nanocarbons, Beijing National Laboratory for Molecular Sciences, College of Chemistry and Molecular Engineering, Peking University, Beijing 100871, P.R. China*

**Shishu Zhang** − *Center for Nanochemistry, Beijing Science and Engineering Center for Nanocarbons, Beijing National Laboratory for Molecular Sciences, College of Chemistry and Molecular Engineering, Peking University, Beijing 100871, P.R. China*

**Yuping Shi** − *Center for Nanochemistry, Beijing Science and Engineering Center for Nanocarbons, Beijing National Laboratory for Molecular Sciences, College of Chemistry and Molecular Engineering and Department of Materials Science and Engineering, College of Engineering, Peking University, Beijing 100871, P.R. China*

**Yanfeng Zhang** − *Center for Nanochemistry, Beijing Science and Engineering Center for Nanocarbons, Beijing National Laboratory for Molecular Sciences, College of Chemistry and Molecular Engineering and Department of Materials Science and Engineering, College of Engineering, Peking University, Beijing 100871, P.R. China;* orcid.org/0000-0003-1319-3270

**Riichiro Saito** − *Department of Physics, Tohoku University, Sendai 980-8578, Japan;* orcid.org/0000-0002-3336-9985

**Jin Zhang** − *Center for Nanochemistry, Beijing Science and Engineering Center for Nanocarbons, Beijing National Laboratory for Molecular Sciences, College of Chemistry and Molecular Engineering, Peking University, Beijing 100871, P.R. China;* orcid.org/0000-0003-3731-8859

Complete contact information is available at: https://pubs.acs.org/10.1021/acsnano.0c04467


### Author Contributions

Y.Z. conceived the idea and designed the experiments. S.Z. coordinated the measurement of helicity-resolved Raman spectra. Y.S. and Y.Z. provided the CVD grown $MoS_2$. Y.Z., L.T., and R.S. wrote the manuscript. R.S. proposed the present experiments and discussion on the helicity selection rule of $MoS_2$. The work was supervised by L.T. and J.Z. All of the authors discussed the results and commented on the manuscript.

### Notes

The authors declare no competing financial interest.

## ACKNOWLEDGMENTS

We thank Xiaobo Li for assistance with ALD experiments, Jianfeng Jiang for assistance with the graphic design, and Prof. Weikun Ge for valuable discussions. This work was financially supported by the Beijing National Laboratory for Molecular Sciences (BNLMS-CXTD-202001), the Ministry of Science and Technology of China (2016YFA0200104 and 2018YFA0703502), and the National Natural Science Foundation of China (Grant Nos. 51720105003, 21790052, 21573004, 21974004, and 51991344). R.S. acknowledges JSPS KAKENHI (Grant No. JP18H01810).

## REFERENCES

(1) Zhang, X.; Qiao, X.-F.; Shi, W.; Wu, J.-B.; Jiang, D.-S.; Tan, P.-H. Phonon and Raman Scattering of Two-Dimensional Transition Metal Dichalcogenides from Monolayer, Multilayer to Bulk Material. *Chem. Soc. Rev.* **2015**, *44*, 2757−2785.

(2) Zhang, S.; Zhang, N.; Zhao, Y.; Cheng, T.; Li, X.; Feng, R.; Xu, H.; Liu, Z.; Zhang, J.; Tong, L. Spotting the Differences in Two-Dimensional Materials - The Raman Scattering Perspective. *Chem. Soc. Rev.* **2018**, *47*, 3217−3240.

(3) Lee, C.; Yan, H.; Brus, L. E.; Heinz, T. F.; Hone, J.; Ryu, S. Anomalous Lattice Vibrations of Single- and Few-Layer $MoS_2$. *ACS Nano* **2010**, *4*, 2695−2700.
(4) Saito, R.; Nugraha, A. R. T.; Hasdeo, E. H.; Siregar, S.; Guo, H.; Yang, T. Ultraviolet Raman Spectroscopy of Graphene and Transition-Metal Dichalcogenides. *Phys. Status Solidi B* **2015**, *252*, 2363−2374.
(5) Lee, C.; Jeong, B. G.; Yun, S. J.; Lee, Y. H.; Lee, S. M.; Jeong, M. S. Unveiling Defect-Related Raman Mode of Monolayer $WS_2$ *via* Tip-Enhanced Resonance Raman Scattering. *ACS Nano* **2018**, *12*, 9982−9990.
(6) Wu, J.; Mao, N.; Xie, L.; Xu, H.; Zhang, J. Identifying the Crystalline Orientation of Black Phosphorus Using Angle-Resolved Polarized Raman Spectroscopy. *Angew. Chem., Int. Ed.* **2015**, *54*, 2366−2369.
(7) Zhang, S.; Mao, N.; Zhang, N.; Wu, J.; Tong, L.; Zhang, J. Anomalous Polarized Raman Scattering and Large Circular Intensity Differential in Layered Triclinic $ReS_2$. *ACS Nano* **2017**, *11*, 10366−10372.
(8) Beams, R.; Cancado, L. G.; Krylyuk, S.; Kalish, I.; Kalanyan, B.; Singh, A. K.; Choudhary, K.; Bruma, A.; Vora, P. M.; Tavazza, F.; Davydov, A. V.; Stranick, S. J. Characterization of Few-Layer 1T' $MoTe_2$ by Polarization-Resolved Second Harmonic Generation and Raman Scattering. *ACS Nano* **2016**, *10*, 9626−9636.
(9) Yu, Z.; Ong, Z.-Y.; Li, S.; Xu, J.-B.; Zhang, G.; Zhang, Y.-W.; Shi, Y.; Wang, X. Analyzing the Carrier Mobility in Transition-Metal Dichalcogenide $MoS_2$ Field-Effect Transistors. *Adv. Funct. Mater.* **2017**, *27*, 1604093.
(10) Kaasbjerg, K.; Thygesen, K. S.; Jacobsen, K. W. Phonon-Limited Mobility in *n*-Type Single-Layer $MoS_2$ from First Principles. *Phys. Rev. B: Condens. Matter Mater. Phys.* **2012**, *85*, 115317.
(11) Sohier, T.; Calandra, M.; Mauri, F. Two-Dimensional Fröhlich Interaction in Transition-Metal Dichalcogenide Monolayers: Theoretical Modeling and First-Principles Calculations. *Phys. Rev. B: Condens. Matter Mater. Phys.* **2016**, *94*, 085415.
(12) Bardeen, J.; Shockley, W. Deformation Potentials and Mobilities in Non-Polar Crystals. *Phys. Rev.* **1950**, *80*, 72−80.
(13) Frohlich, H. Interaction of Electrons with Lattice Vibrations. *Proc. R. Soc. London A* **1952**, *215*, 291−298.
(14) Martin, R. M.; Damen, T. C. Breakdown of Selection Rules in Resonance Raman Scattering. *Phys. Rev. Lett.* **1971**, *26*, 86−88.
(15) Cantarero, A.; Trallero-Giner, C.; Cardona, M. Excitons in One-Phonon Resonant Raman Scattering: Fröhlich and Interference Effects. *Phys. Rev. B: Condens. Matter Mater. Phys.* **1989**, *40*, 12290−12295.
(16) Trallero-Giner, C.; Cantarero, A.; Cardona, M. One-Phonon Resonant Raman Scattering: Fröhlich Exciton-Phonon Interaction. *Phys. Rev. B: Condens. Matter Mater. Phys.* **1989**, *40*, 4030−4036.
(17) Miller, B.; Lindlau, J.; Bommert, M.; Neumann, A.; Yamaguchi, H.; Holleitner, A.; Hoegele, A.; Wurstbauer, U. Tuning the Fröhlich Exciton-Phonon Scattering in Monolayer $MoS_2$. *Nat. Commun.* **2019**, *10*, 807.
(18) Mak, K. F.; He, K.; Shan, J.; Heinz, T. F. Control of Valley Polarization in Monolayer $MoS_2$ by Optical Helicity. *Nat. Nanotechnol.* **2012**, *7*, 494−498.
(19) Schaibley, J. R.; Yu, H.; Clark, G.; Rivera, P.; Ross, J. S.; Seyler, K. L.; Yao, W.; Xu, X. Valleytronics in 2D Materials. *Nat. Rev. Mater.* **2016**, *1*, 16055.
(20) Chen, S.-Y.; Zheng, C.; Fuhrer, M. S.; Yan, J. Helicity-Resolved Raman Scattering of $MoS_2$, $MoSe_2$, $WS_2$, and $WSe_2$ Atomic Layers. *Nano Lett.* **2015**, *15*, 2526−2532.
(21) Drapcho, S. G.; Kim, J.; Hong, X.; Jin, C.; Shi, S.; Tongay, S.; Wu, J.; Wang, F. Apparent Breakdown of Raman Selection Rule at Valley Exciton Resonances in Monolayer $MoS_2$. *Phys. Rev. B: Condens. Matter Mater. Phys.* **2017**, *95*, 165417.
(22) Yoshikawa, N.; Tani, S.; Tanaka, K. Raman-Like Resonant Secondary Emission Causes Valley Coherence in CVD-Grown Monolayer $MoS_2$. *Phys. Rev. B: Condens. Matter Mater. Phys.* **2017**, *95*, 115419.
(23) Tatsumi, Y.; Kaneko, T.; Saito, R. Conservation Law of Angular Momentum in Helicity-Dependent Raman and Rayleigh Scattering. *Phys. Rev. B: Condens. Matter Mater. Phys.* **2018**, *97*, 195444.
(24) Martin, R. M. Theory of the One-Phonon Resonance Raman Effect. *Phys. Rev. B* **1971**, *4*, 3676−3685.
(25) Coehoorn, R.; Haas, C.; Dijkstra, J.; Flipse, C. J.; de Groot, R. A.; Wold, A. Electronic Structure of $MoSe_2$, $MoS_2$, and $WSe_2$. I. Band-Structure Calculations and Photoelectron Spectroscopy. *Phys. Rev. B: Condens. Matter Mater. Phys.* **1987**, *35*, 6195−6202.
(26) Zhu, Z. Y.; Cheng, Y. C.; Schwingenschlögl, U. Giant Spin-Orbit-Induced Spin Splitting in Two-Dimensional Transition-Metal Dichalcogenide Semiconductors. *Phys. Rev. B: Condens. Matter Mater. Phys.* **2011**, *84*, 153402.
(27) Splendiani, A.; Sun, L.; Zhang, Y.; Li, T.; Kim, J.; Chim, C.-Y.; Galli, G.; Wang, F. Emerging Photoluminescence in Monolayer $MoS_2$. *Nano Lett.* **2010**, *10*, 1271−1275.
(28) Molina-Sanchez, A.; Wirtz, L. Phonons in Single-Layer and Few-Layer $MoS_2$ and $WS_2$. *Phys. Rev. B: Condens. Matter Mater. Phys.* **2011**, *84*, 155413.
(29) Zhang, L.; Niu, Q. Chiral Phonons at High-Symmetry Points in Monolayer Hexagonal Lattices. *Phys. Rev. Lett.* **2015**, *115*, 115502.
(30) Tatsumi, Y.; Saito, R. Interplay of Valley Selection and Helicity Exchange of Light in Raman Scattering for Graphene and $MoS_2$. *Phys. Rev. B: Condens. Matter Mater. Phys.* **2018**, *97*, 115407.
(31) Cantarero, A.; Trallero-Giner, C.; Cardona, M. Excitons in One-Phonon Resonant Raman Scattering: Deformation-Potential Interaction. *Phys. Rev. B: Condens. Matter Mater. Phys.* **1989**, *39*, 8388−8397.
(32) O'Donnell, K. P.; Chen, X. Temperature Dependence of Semiconductor Band Gaps. *Appl. Phys. Lett.* **1991**, *58*, 2924−2926.
(33) Chen, Y.; Wen, W.; Zhu, Y.; Mao, N.; Feng, Q.; Zhang, M.; Hsu, H. P.; Zhang, J.; Huang, Y. S.; Xie, L. Temperature-Dependent Photoluminescence Emission and Raman Scattering from $Mo_{1-x}W_xS_2$ Monolayers. *Nanotechnology* **2016**, *27*, 445705.
(34) Raja, A.; Waldecker, L.; Zipfel, J.; Cho, Y.; Brem, S.; Ziegler, J. D.; Kulig, M.; Taniguchi, T.; Watanabe, K.; Malic, E.; Heinz, T. F.; Berkelbach, T. C.; Chernikov, A. Dielectric Disorder in Two-Dimensional Materials. *Nat. Nanotechnol.* **2019**, *14*, 832−837.
(35) Lin, Y.; Ling, X.; Yu, L.; Huang, S.; Hsu, A. L.; Lee, Y. H.; Kong, J.; Dresselhaus, M. S.; Palacios, T. Dielectric Screening of Excitons and Trions in Single-Layer $MoS_2$. *Nano Lett.* **2014**, *14*, 5569−5576.
(36) Komsa, H.-P.; Krasheninnikov, A. V. Effects of Confinement and Environment on the Electronic Structure and Exciton Binding Energy of $MoS_2$ from First Principles. *Phys. Rev. B: Condens. Matter Mater. Phys.* **2012**, *86*, 241201.
(37) Jiang, J.; Saito, R.; Samsonidze, G. G.; Jorio, A.; Chou, S. G.; Dresselhaus, G.; Dresselhaus, M. S. Chirality Dependence of Exciton Effects in Single-Wall Carbon Nanotubes: Tight-Binding Model. *Phys. Rev. B: Condens. Matter Mater. Phys.* **2007**, *75*, 035407.
(38) Jiang, J.; Saito, R.; Sato, K.; Park, J. S.; Samsonidze, G. G.; Jorio, A.; Dresselhaus, G.; Dresselhaus, M. S. Exciton-Photon, Exciton-Phonon Matrix Elements, and Resonant Raman Intensity of Single-Wall Carbon Nanotubes. *Phys. Rev. B: Condens. Matter Mater. Phys.* **2007**, *75*, 035405.
(39) Laturia, A.; Van de Put, M. L.; Vandenberghe, W. G. Dielectric Properties of Hexagonal Boron Nitride and Transition Metal Dichalcogenides: From Monolayer to Bulk. *npj 2D Mater. Appl.* **2018**, *2*, 6.
(40) Li, Q.; Huang, S.; Pan, D.; Wang, J.; Zhao, J.; Xu, H. Q. Suspended InAs Nanowire Gate-All-Around Field-Effect Transistors. *Appl. Phys. Lett.* **2014**, *105*, 113106.
(41) Santos, E. J. G.; Kaxiras, E. Electrically Driven Tuning of the Dielectric Constant in $MoS_2$ Layers. *ACS Nano* **2013**, *7*, 10741−10746.
(42) Zhu, Y.; Xie, J.; Pei, A.; Liu, B.; Wu, Y.; Lin, D.; Li, J.; Wang, H.; Chen, H.; Xu, J.; Yang, A.; Wu, C. L.; Wang, H.; Chen, W.; Cui, Y. Fast Lithium Growth and Short Circuit Induced by Localized-


https://dx.doi.org/10.1021/acsnano.0c04467
*ACS Nano* 2020, 14, 10527−10535

Temperature Hotspots in Lithium Batteries. *Nat. Commun.* **2019**, *10*, 2067.

(43) Yan, R.; Simpson, J. R.; Bertolazzi, S.; Brivio, J.; Watson, M.; Wu, X.; Kis, A.; Luo, T.; Walker, A. R. H.; Xing, H. G. Thermal Conductivity of Monolayer Molybdenum Disulfide Obtained from Temperature-Dependent Raman Spectroscopy. *ACS Nano* **2014**, *8*, 986−993.

(44) Mitioglu, A. A.; Plochocka, P.; Jadczak, J. N.; Escoffier, W.; Rikken, G. L. J. A.; Kulyuk, L.; Maude, D. K. Optical Manipulation of the Exciton Charge State in Single-Layer Tungsten Disulfide. *Phys. Rev. B: Condens. Matter Mater. Phys.* **2013**, *88*, 245403.



https://dx.doi.org/10.1021/acsnano.0c04467
*ACS Nano* 2020, 14, 10527−10535